Probing the densities of the Sn isotopes

K. Amos*

School of Physics, University of Melbourne, Victoria 3010, Australia

S. Karataglidis†

Theoretical Division, Los Alamos National Laboratory, Los Alamos, New Mexico, 87545

J. Dobaczewski‡

Institute of Theoretical Physics, Warsaw University, PL-00-681, Warsaw, Poland

(Dated: May 6, 2002)

Abstract

Proton and neutron densities have been obtained for the even-even isotopes of Sn from ^{100}Sn to ^{176}Sn using a Hartree-Fock-Bogoliubov model with a Skyrme interaction. The matter densities so defined have been used with realistic nucleon-nucleon interactions in a folding model to specify optical potentials for the elastic scattering of 65 and 200 MeV protons from which predictions of the differential cross sections and spin observables result. As mass increases, one observes the emergence of the neutron skin in the Sn isotopes whose effect on the differential cross section is marked. Comparisons with available data show how scattering data for the neutron-rich isotopes is likely to provide constraints for the model structures.

PACS numbers: 21.10.Gv,24.10.Ht,25.40.Cm

*Electronic address: `amos@physics.unimelb.edu.au`
†Electronic address: `stevenk@lanl.gov`
‡Electronic address: `Jacek.Dobaczewski@fuw.edu.pl`

I. INTRODUCTION

One of the goals of modern nuclear physics is to understand the structures of nuclei far from the line of stability and at extremes of isospin. Thus far such studies have largely dealt with the light nuclei for which radioactive beams have been available at facilities such as TRIUMF/ISAC, NSCL, RIKEN, and CERN/ISOLDE. Early experiments have lead to the identification of novel structures of which the halo [1] is the best known after its identification in ^{11}Li. In light of projected experimental facilities using radioactive ion beams to extend such investigations to heavy nuclei, there have been advances in the theoretical study of neutron rich nuclei across the whole mass range (see refs. [1–5] for reviews). Studies of such nuclei have topical interest since nuclei far from stability play an important role in nucleosynthesis with short-lived species formed as part of the r- and rp- processes. The structures of those nuclei determine the rates at which the nucleon-capture reactions proceed against the interplay of weak decays and photo-disintegration and thus are key elements in the determination of the abundances of stable nuclei in the universe.

Of course, these exotic systems are of interest in their own right given that they may exhibit forms of nuclear matter quite different from that known with the stable isotopes. Of particular interest are the separate density distributions of proton and neutrons. As well as halos, heavier systems may lead to the identification of pronounced neutron skins [6] and/or to dramatic changes in the nuclear shell structure [7].

An important observable by which the model structures are tested is the ground state density. For stable nuclei, one usually seeks a measure of that from the elastic scattering of electrons which measures the charge and current densities from the longitudinal and transverse form factors, respectively. To complement that information, which primarily focuses on the proton density itself, one looks to the elastic scattering of nucleons from nuclei which measures the matter density. As the effective nucleon-nucleon (NN) interaction is dominated by the isoscalar $^3S_1$ channel, proton scattering predominantly measures the neutron density and *vice versa*. For radioactive nuclei, the only available measure of the ground state density comes from the scattering of nuclei from hydrogen which, in the inverse kinematics, corresponds to proton scattering. However, to gauge the validity of the structure model from which the density is obtained, a model of scattering which is able to predict the scattering observables and is sensitive to changes in the density is required.

For nuclei above the fp-shell, mean-field models of structure are at the forefront of current studies of the ground state densities. Usually those calculations are made in a relativistic Hartree or Hartree-Fock model [8–11] or a non-relativistic Skyrme-Hartree-Fock-Bogoliubov model [12–14]. This mean-field approach works as the ground state properties for heavy nuclei arise more generally from the bulk properties of the density as opposed to single particle properties. As one approaches the drip lines, however, surface properties become more important and, in concert, so do single particle densities.

A test case has been to use nucleon elastic scattering to determine/extract the neutron skin thickness in ^{208}Pb. Karataglidis *et al.* [15] have shown that the differential cross sections from the elastic scattering of 200 MeV protons from ^{208}Pb suggests a neutron skin thickness in the nucleus of ~ 0.17 fm. More importantly, that study also showed that such scattering analyzes could select between disparate model structures that had the same root mean square (rms) radii. By itself, the rms radius is not an adequate indicator of the validity of a model structure. To use the scattering data to differentiate between models of structure, a predictive theory of nucleon-nucleus (NA) scattering was needed. Just such has been developed in the past decade [16]. That theory is *direct* in that all quantities required are defined *a priori* with no *a posteriori* adjustment of results. With the nucleus viewed as a system of A nucleons, NA scattering is determined by an optical potential formed by a folding process. That folding requires use of realistic interactions of the projectile with each and every nucleon constituting the ground state target density. Such microscopic approaches defining the NA optical potential have been quite successful in predicting both angle-dependent and integral observables of elastic scattering [16, 17]. In the coordinate space approach, and for analyzes that use the DWBA98 programs [18], the projectile-target nucleon interaction not only is complex but also it is energy dependent and non-local. We have used that program to calculate cross sections for the scattering of all the even mass isotopes $^{100-176}$Sn from hydrogen at an energy of $200A$ MeV using optical potentials formed by folding realistic effective NN interactions with the details of densities of those nuclei given by the mean-field models of their structure. With optical potentials so formed previously, differential cross sections and spin observables for proton scattering at 200 MeV specifically and from diverse targets ranging from ^{3}He to ^{238}U have been predicted and found to agree very well with data. The complex (non-local) optical potentials are formed by folding effective interactions determined from NN g matrices [solutions of Brueckner-Bethe-Goldstone (BBG) equations for nuclear matter] found from realistic free NN forces. Details of the specifications of those effective NN interactions, of the folding process that gives the optical potential, and of the successful predictions of differential cross sections and analyzing powers from the scattering of protons at diverse energies and from diverse mass targets, have been summarized before [16] and so are not repeated herein.

In the next section, we outline the structure models used in our scattering calculations and present therein details of the proton and neutron matter distributions generated therefrom. In Section III we show the results found using those structures and an established effective NN force in nuclear matter in generating g-folding optical potentials for a wide range of Sn isotopes scattering from hydrogen. An energy of $200A$ MeV has been used. In Section IV application of structure and scattering models is made for two cases (^{118,120}Sn) for which proton elastic scattering data are available. Conclusions are presented in Section V.

II. MODELS OF STRUCTURE OF THE SN ISOTOPES

In the present study, the properties of even-even Sn isotopes (masses 100 to 176) are described using the spherical mean-field Hartree-Fock-Bogoliubov (HFB) model [12]. Two Skyrme interactions have been used. As a description of the method has been given in detail elsewhere [14, 19, 20]; only details pertaining to the particular calculations made and used herein are given. We have used two parameterizations of the Skyrme force, SkP [19] and SLy4 [21], that are known to give a correct description of bulk nuclear properties. They differ by the input values of the nuclear-matter effective mass, being $m^*/m = 1$ and 0.7 respectively. The zero-range density-dependent pairing force was used in the particle-particle channel, with the form that is intermediate between volume and surface attraction [14]. A large positive energy phase space of 60 MeV was taken and for which the pairing-force strengths of $V_0 = -286.20$ and -212.94 MeV fm^{-3} were obtained in the SkP and SLy4 cases respectively. Those strengths result on using a standard adjustment [22] of the neutron pairing gap in ^{120}Sn. In Fig. 1 we compare with data, the two-neutron separation energies S_{2N} and the neutron pairing gaps Δ_N calculated from the two HFB models so that the quality of the description of the Sn isotopes may be judged. Experimental pairing gaps of even-N isotopes

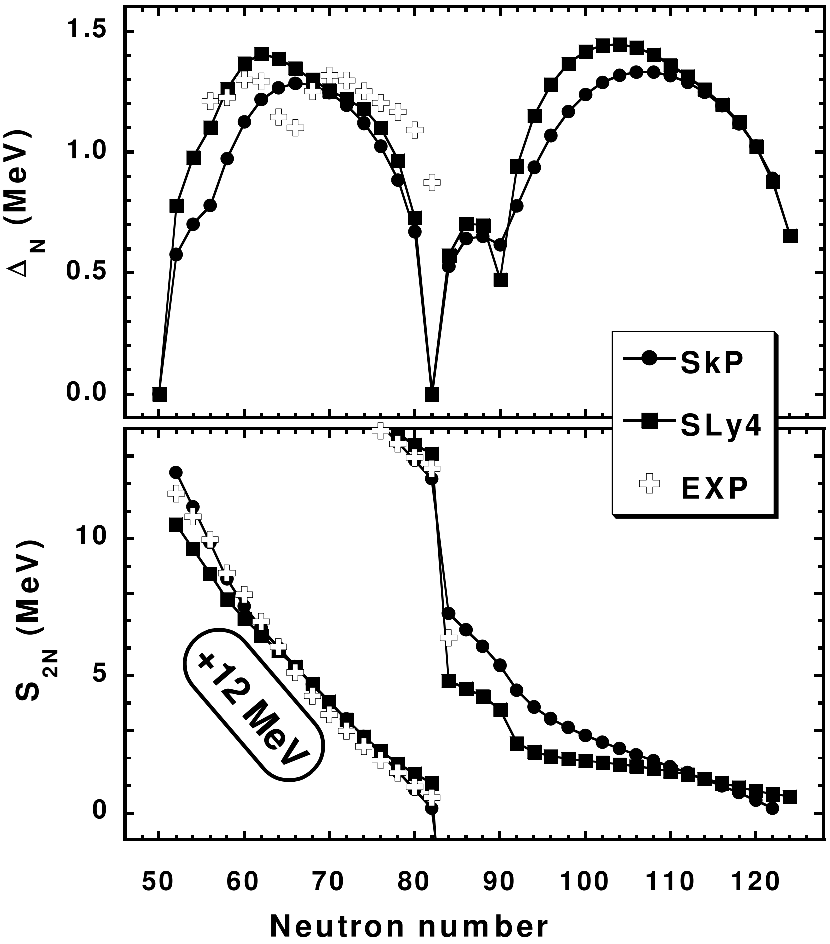

FIG. 1: Two-neutron separation energies S_{2N} (lower) and the neutron pairing gaps Δ_N (upper) obtained within the HFB/SkP and HFB/SLy4 models compared with experimental data.

were estimated from the nuclear masses [23] as averages $\left[\Delta^{(3)}(N-1)+\Delta^{(3)}(N+1)\right]/2$ of the three-point staggering parameters [24] centered at odd neutron numbers $(N-1)$ and $(N+1)$. Evidently a fairly good description of pairing properties is obtained in between the magic numbers $N=50$ and $N=82$. At the magic numbers, the calculated gaps vanish due to the known effect of an unphysical, too sudden, pairing phase transition. The size of the jump of S_{2N} at $N=82$ is slightly underestimated (overestimated) by the HFB/SkP (SLy4) model. That is an effect of the different values of the effective mass. Nevertheless, the overall quality of agreement between theory and experiment suffices for us to consider the two models to be useful for extrapolations to describe unknown heavy Sn isotopes.

Spatial properties of neutron and proton density distributions are of special interest in a number of contexts. With structure studies, geometric aspects have been found in the past [6] by using the Helm model. Using those methods, four quantities are summarized in Figs. 2 and 3. Results are shown for all even Sn isotopes between $N=50$ and the two-neutron drip line ($N=122$ and $N=124$ for SkP and SLy4, respectively). These presentations are of the bulk (interior) particle density, $\rho_{\rm bulk}$, the diffraction radius, R_0, the surface thickness, σ, and neutron skin thickness, $\delta R_{\rm skin}$, as often sought from the microscopically calculated densities $\rho(r)$. R_0 and σ were obtained by comparing positions of the first zero and first maximum

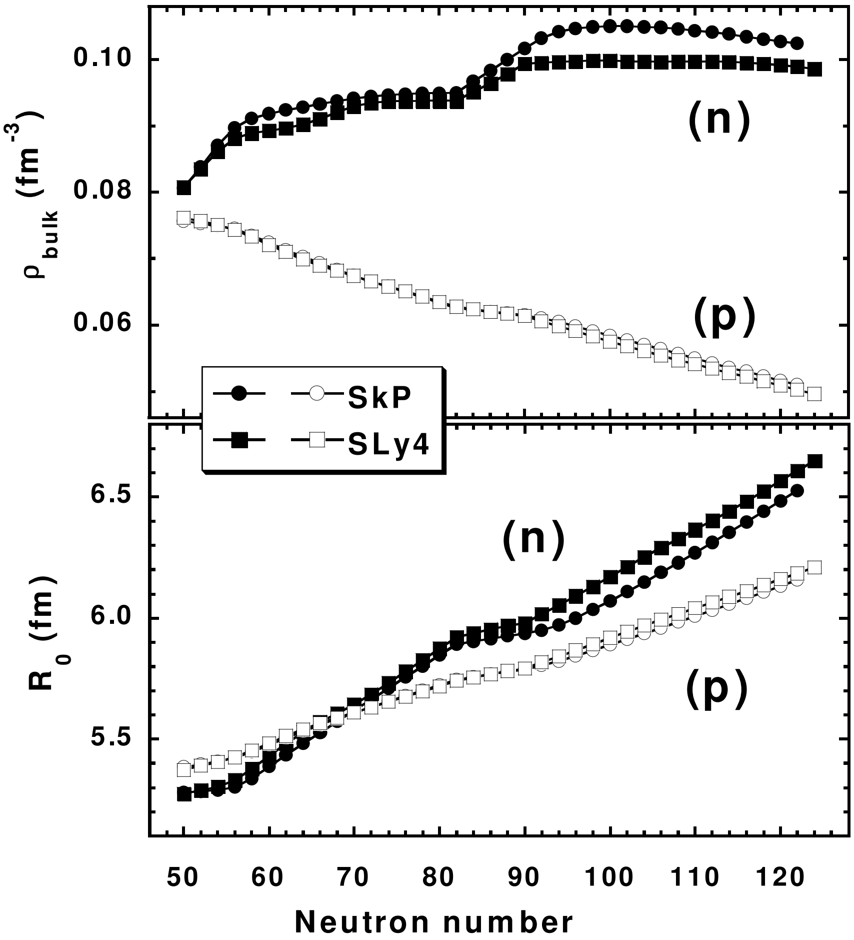

FIG. 2: Calculated neutron (filled symbols) and proton (open symbols) diffraction radii (lower) and bulk densities (upper). Circles and squares correspond to the results obtained within the HFB/SkP and HFB/SLy4 models respectively.

of the microscopic and Helm model form factors. The neutron skin thickness is identified as the difference between neutron and proton Helm radii, $R_{\rm Helm} = \sqrt{R_0^2 + 5\sigma^2}$. Finally, $\rho_{\rm bulk}$ was obtained by calculating the average microscopic density $\langle\rho\rangle = 4\pi \int r^2\rho^2(r)/A$, and identifying it with the analogous value for the Helm model density in which $\rho_{\rm bulk}$ is a parameter.

Certain features of the calculated HFB neutron and proton densities in the Sn isotopes are readily apparent in these figures. With increasing number of neutrons, the neutron and proton radii increase at different rates; the neutron radii being the faster. As a result there is a gradual increase in the size of the neutron skin; an increase that is almost linear with neutron number. At the same time the neutron and proton bulk densities increase and decrease, respectively. The balance between the bulk and surface increase of the neutron distribution is governed by the volume and surface attractions between neutrons and protons and hence is fixed by the principal features of the volume and surface terms in nuclear masses. Since these are rigidly adjusted to experimental data, the net results obtained with both Skyrme interactions, as expected, are quite similar. Note also from Fig. 3, that the surface thickness of the neutron distributions defined in this way increases by about 50% across

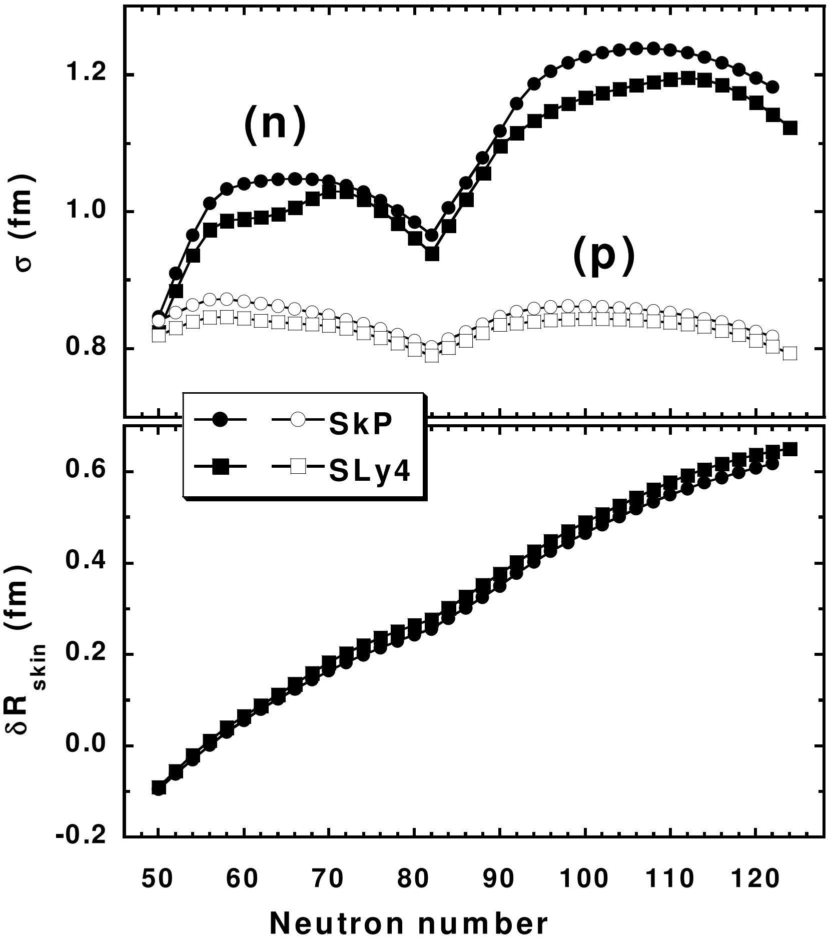

FIG. 3: Same as in Fig. 2, but for the neutron skins (lower) and surface thicknesses (upper).

the nuclear chart while that of protons stays almost constant, apart from very visible shell fluctuations created by the analogous effects in the neutrons.

Alternative to the above approach is inspection of the actual density profiles deduced from the shell occupancies and associate canonical wave functions of the mean-field model results. Such complete density distributions for all of the even mass Sn isotopes resulting from the SLy4 and SkP models of their structure are so shown in Figs. 4 through 9. Using the SLy4 force, the proton and neutron matter distributions for all even mass Sn isotopes resulting from the mean-field calculations are displayed in Figs. 4 and 5 respectively. The proton (neutron) distributions are plotted with nuclear mass decreasing (increasing) into the page. By that means the variations to those densities are best portrayed in block form. The proton number of course is fixed at 50 and so as the neutron number increases, and concomitantly the neutron volume increases, those 50 protons extend over an increasing volume. As noted above that is due to the strong attractive neutron-proton interactions. In concert, the central charge density must, and does, decrease. However, and as will be seen more clearly in Fig. 8 below, the charge distributions do not become significantly more diffuse. The prime effect is the $\sim 33\%$ increase in the charge volume.

The neutron densities generated using the SLy4 model have a different structure variation with increasing mass. The general trend that the neutron rms radii increase is evident as the

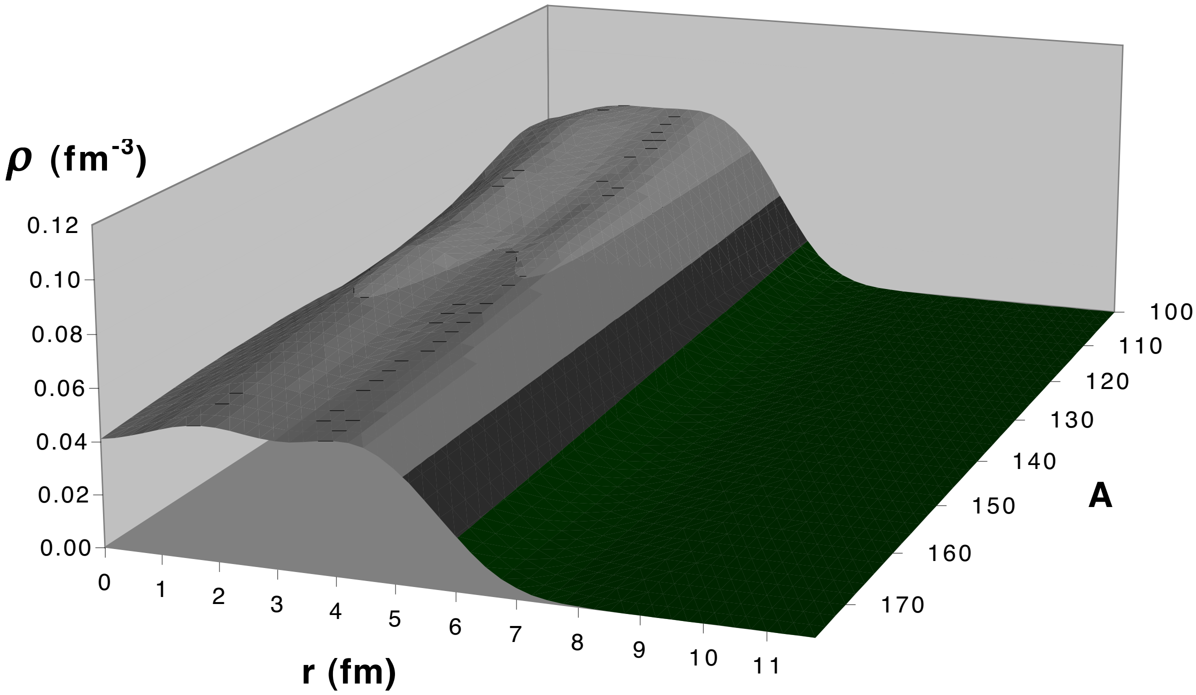

FIG. 4: The proton density mass variation from the SLy4 model of structure for the Sn isotopes.

half central density is reached at radii ranging from ~ 5 fm in ^{100}Sn to ~ 6.5 fm for ^{170}Sn. The increase of the neutron surface diffuseness is difficult to see from a direct inspection of the density profiles, although it is evident in the results shown in Fig. 3. We note also that a strong oscillation develops in the central density, which on average also increases from ~ 0.08 neutrons/fm^3 in ^{100}Sn to ~ 0.1 neutrons/fm^3 for ^{170}Sn.

The features identified above also are evident in the results found using the SkP force in the HFB calculations. Those results are shown in Figs. 6 and 7 for the protons and neutrons respectively. Again, for clarity, the proton distributions are plotted with mass decreasing into the page. While the prime features of these densities are as observed with the SLy4 model results, there are differences in detail.

The mass variations of densities are evident also in Figs. 8 and 9 wherein the proton and neutron densities respectively for the Sn isotopes calculated using the SLy4 model are given for a select set of 8 nuclei having masses spaced evenly between 100 and 170. In Fig. 8 it is evident that the 50 protons are rearranged to be more extensive as one increases mass. Note that the half-density radius ranges from ~ 5 fm for ^{100}Sn to ~ 6 fm in ^{170}Sn. However the proton surface diffuseness remains essentially unchanged. The distance over which the charge density falls from 90% to 10% of its central value is ~ 2 fm in all nuclei. That is also the case for the neutron distributions. There is a gradual development of a neutron skin to the Sn isotopes, for while with ^{100}Sn the 50 protons and 50 neutrons have essentially the same distribution (solid dark lines in the figures), the two density profiles are somewhat disparate in ^{170}Sn. Not only does the neutron central density increase by $\sim 25\%$ from its value in ^{100}Sn while the proton central density value decreases by $\sim 40\%$, but the skin, in this case $R_{rms}(\text{neutron}) - R_{rms}(\text{proton})$, varies from 0 to ~ 0.5 fm as noted previously from the definition in the Helm model characterization.

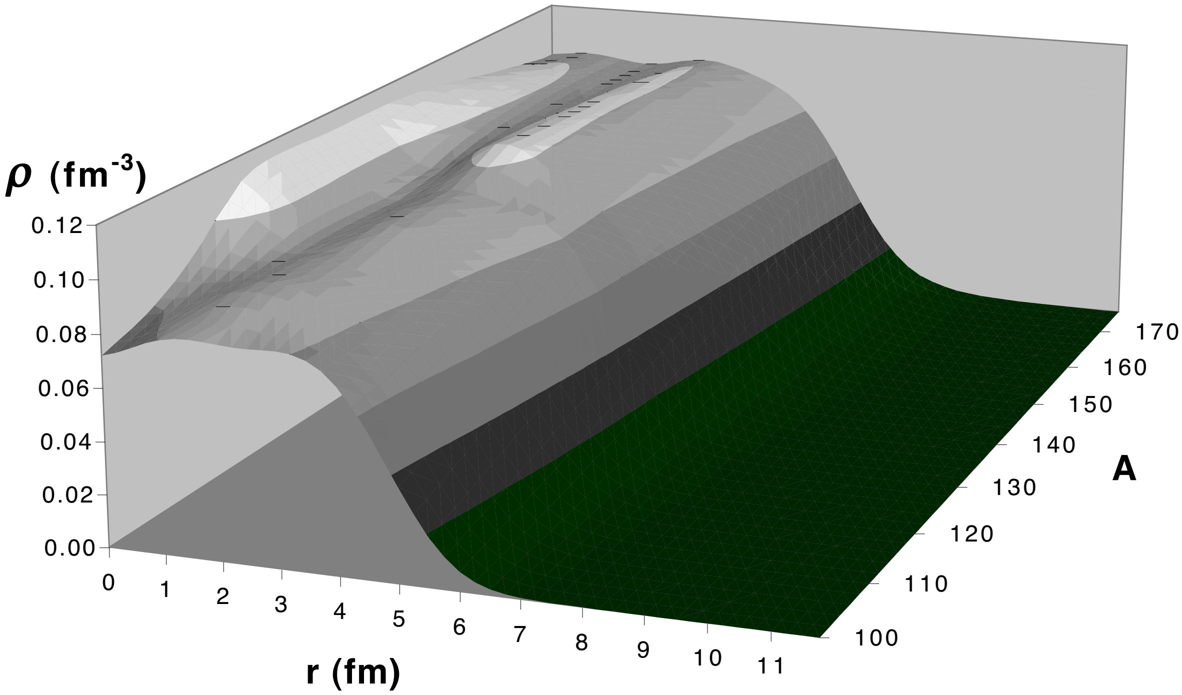

FIG. 5: The neutron density mass variation from the SLy4 model of structure for the Sn isotopes.

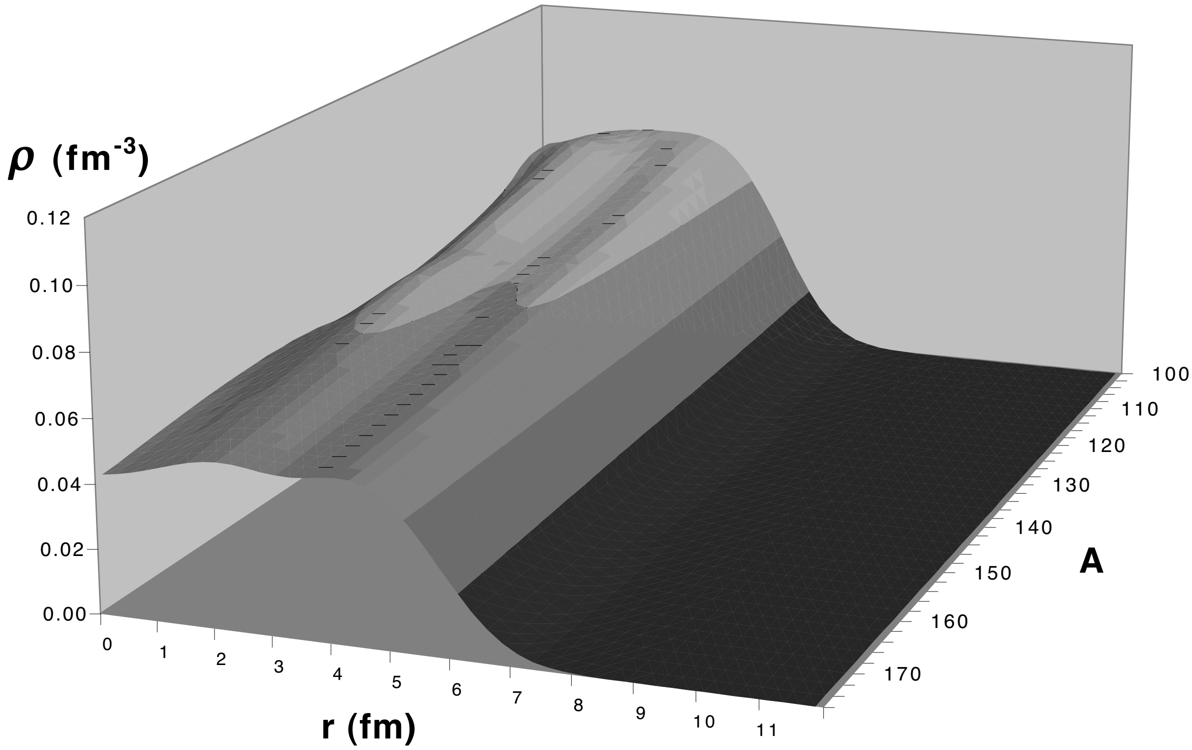

FIG. 6: The proton density mass variation from the SkP model of structure for the Sn isotopes.

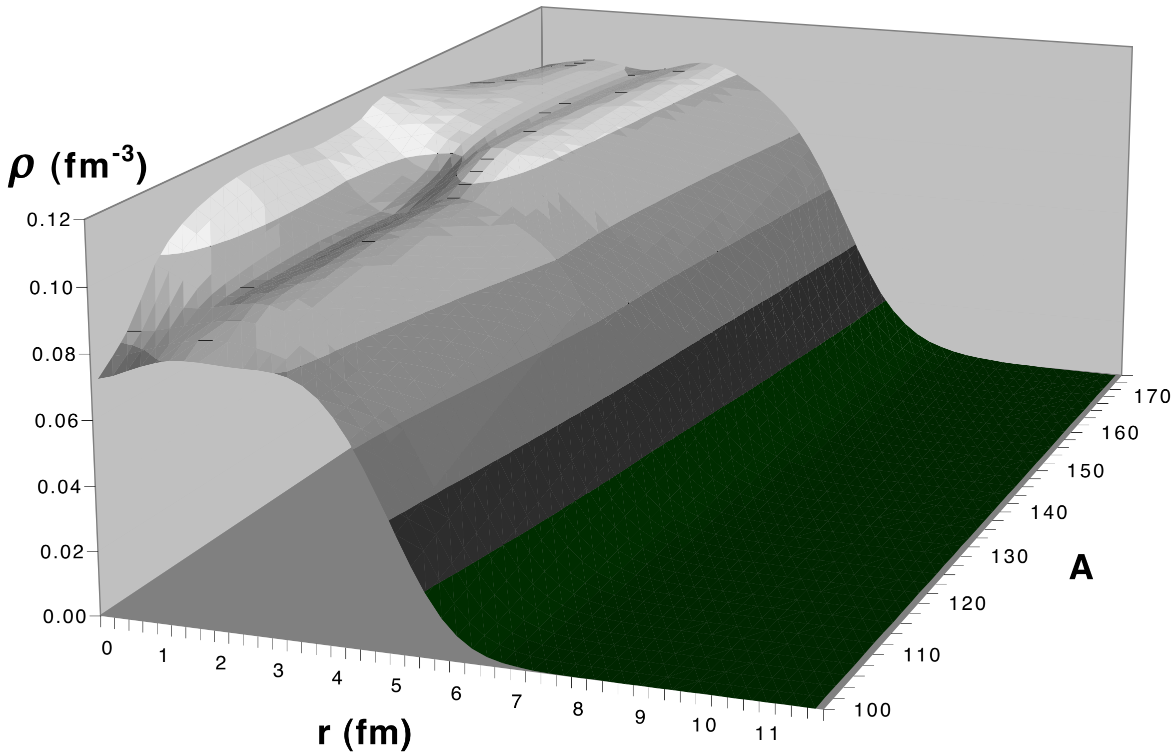

FIG. 7: The neutron density mass variation from the SkP model of structure for the Sn isotopes.

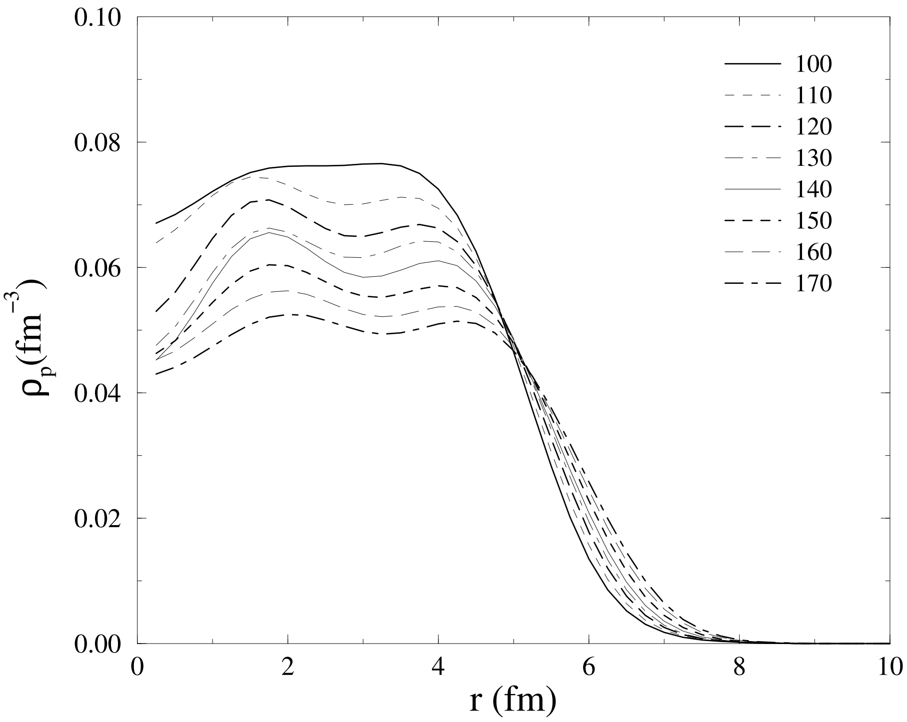

FIG. 8: The proton densities given by the SLy4 model of structure for 8 isotopes of Sn.

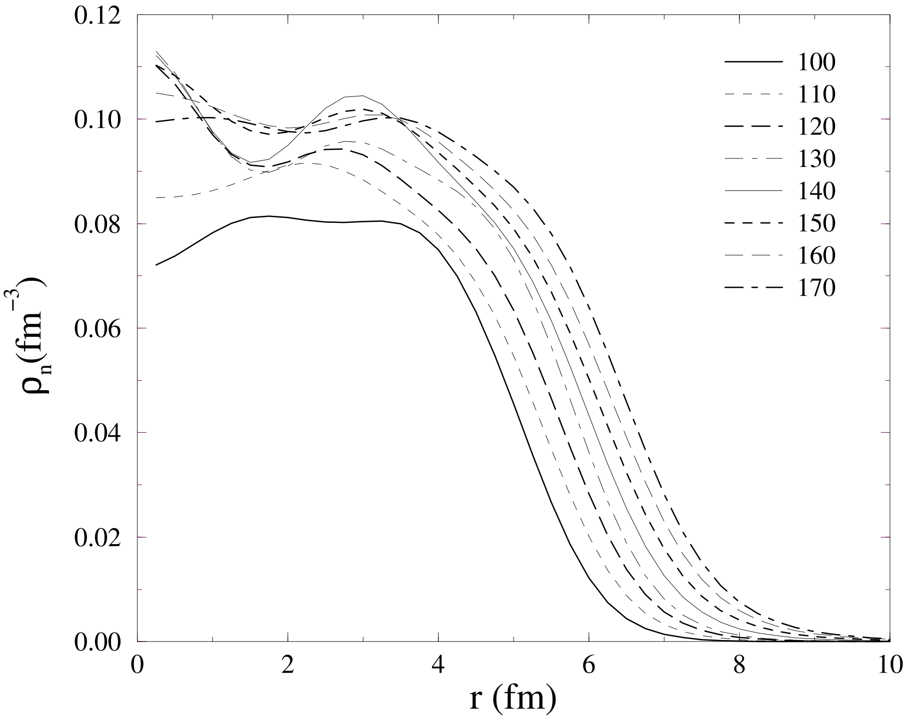

FIG. 9: The neutron densities given by the SLy4 model of structure for 8 isotopes of Sn.

III. SCATTERING FROM HYDROGEN – GEDANKEN RESULTS

We have used the canonical single-particle wave functions for all of the Sn isotopes to fold an effective NN interaction and thus generate optical potentials for use in modified versions of the scattering program DWBA98 [18]. Those optical potentials are complex and non-local since they can be written in coordinate space with $\boldsymbol{r}_{12} = \boldsymbol{r}_1 - \boldsymbol{r}_2$, as

$$U(\boldsymbol{r}_1, \boldsymbol{r}_2; E) = U_D(\boldsymbol{r}_1; E)\,\delta(\boldsymbol{r}_{12}) + U_E(\boldsymbol{r}_1, \boldsymbol{r}_2; E)\ , \tag{1}$$

where the direct U_D and non-local exchange U_E terms are

$$\begin{aligned} U_D &= \sum_n \zeta_n \left\{ \int \varphi_n^*(\boldsymbol{s}) v_D(\boldsymbol{r}_{1s}) \varphi_n(\boldsymbol{s})\, d\boldsymbol{s} \right\} \\ U_E &= \sum_n \zeta_n \left\{ \varphi_n^*(\boldsymbol{r}_1) v_{Ex}(\boldsymbol{r}_{12}) \varphi_n(\boldsymbol{r}_2) \right\}\ . \end{aligned} \tag{2}$$

Here v_D and v_{Ex} are combinations of the components of the effective NN interactions, ζ_n are ground state one body density matrices (effectively bound state shell occupancies), and $\varphi_n(\boldsymbol{s})$ are single nucleon bound states. All details and the prescription of solution of the associated nonlocal Schrödinger equations are given in the recent review [16]. The results to be discussed herein have been obtained by solving the actual nonlocal Schrödinger equations defined with potentials as given by Eq. (1). For the present calculations, the effective NN interactions have been defined by their mapping to the BBG g matrices of the BonnB NN interaction [25].

We consider the elastic scattering of 200 MeV protons from each of the even mass Sn isotopes ($A = 100$ to 176). By inverse kinematics the cross sections we determine are also

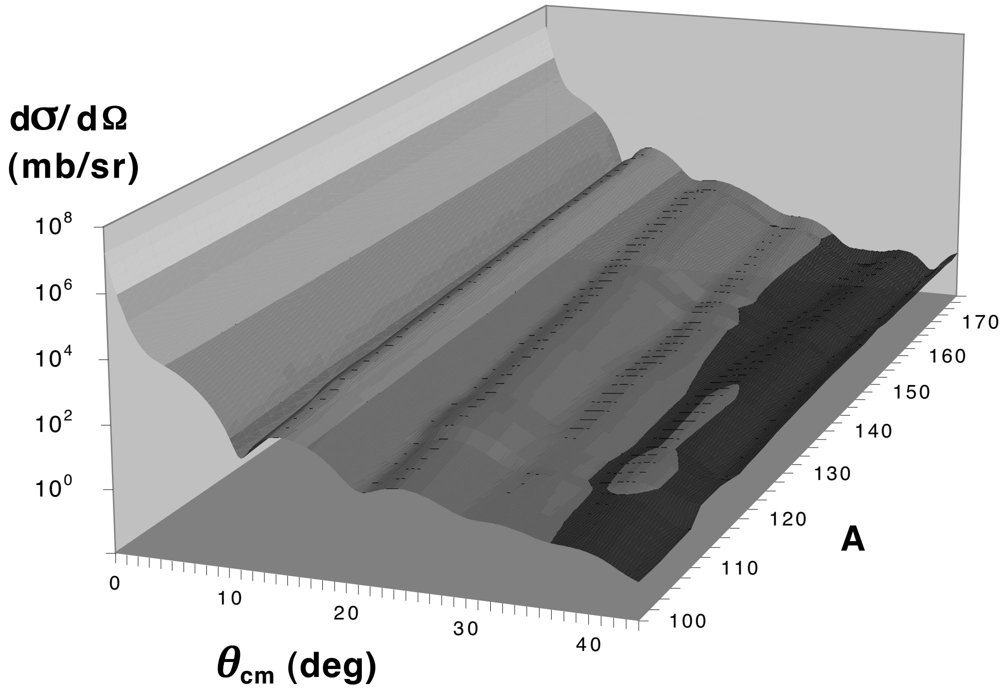

FIG. 10: The differential cross section for the elastic scattering of 200 MeV protons from the Sn isotopes. The SLy4 model was used in forming the optical potentials.

those for the scattering of 200A MeV Sn ions from hydrogen; some of which can be, or may soon be, obtained in sufficient numbers to form a radioactive ion beam for experiment. The choice of 200 MeV was made, not only because the effective force at this energy has been used in many successful predictions of actual scattering data from stable nuclei [16] but also since that energy provided data from ^{208}Pb in which a clear signature of the neutron density profile has been found [15].

In Fig. 10, the differential cross sections for the scattering from all of the even mass Sn isotopes are plotted to 45° in the center of mass by which angle the cross section magnitude is $O(0.1)$ mb/sr. The SLy4 model calculations were used to specify the OBDME and single particle wave functions by which the optical potentials were generated. Several trends are noticed in the differential cross section as the mass is increased. The first three minima tend to forward angles and the intervening (first) maximum becomes more pronounced as the neutron number increases. There are model signatures in these results for scattering angles 30° (and higher) that have magnitudes still possible to be detected in experiment. Since the p-n force (isoscalar $^3S_1$ channel) is the strongest, such effects primarily reflect attributes of the neutron density variation in the surface region of the nuclei. They are revealed also by considering the ratio to Rutherford values which are shown in Fig. 11. Therein the marked change in the magnitudes of results for the isotope in the mass range 110 to 120 as is the trend of peak and valley magnitudes to smaller momentum transfer as mass increases.

If ever exotic Sn nuclei can be formed as a radioactive beam for scattering from polarized hydrogen targets, spin measurables such as the spin rotation, Q, could be found. That quantity from the SLy4 model calculations is shown in Fig. 12. The graphical view has

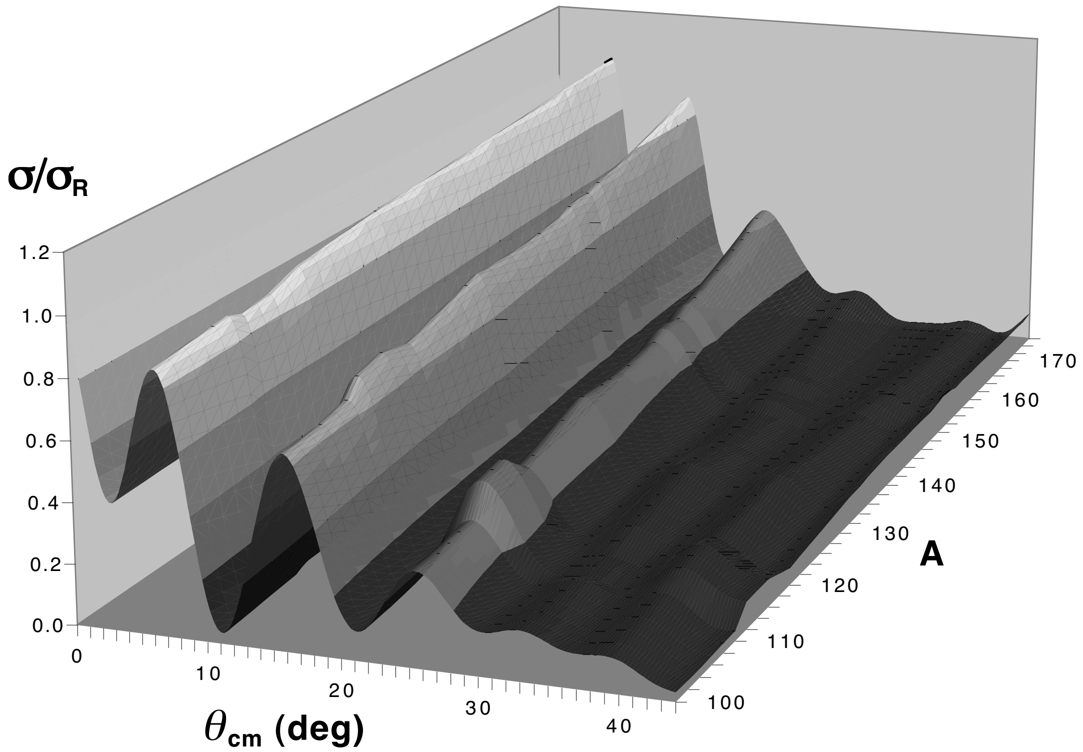

FIG. 11: The results of Fig.10 shown as ratios to Rutherford scattering.

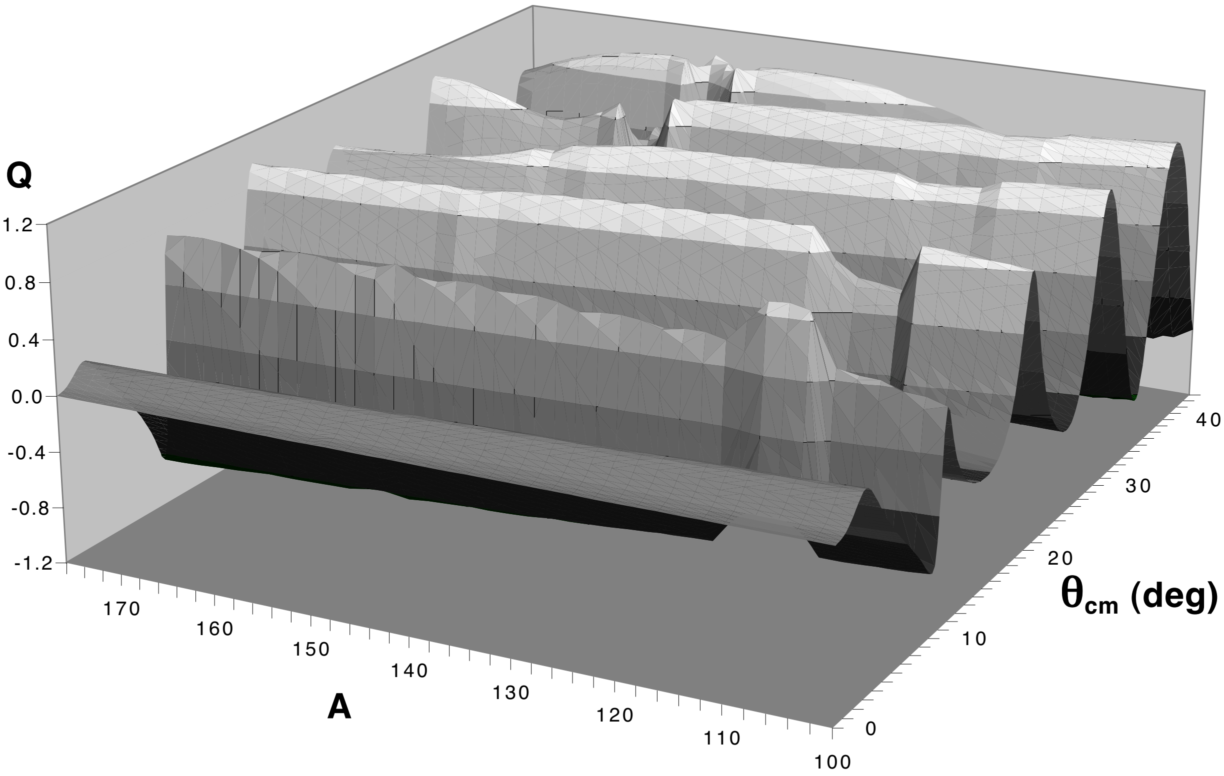

FIG. 12: The spin observable Q from 200 MeV proton scattering with the Sn isotopes.

been rotated from the aspect given with the cross section results to show more readily the model dependencies in our calculated results. For clarity, the mass variation now is shown across the page while the scattering angle variation occurs into the page. Again the prime feature of these results is the trend with mass for the peaks and valleys to smaller momentum transfer values, but there is also a strong model dependence of magnitudes, notably in the mass range 110 to 120.

IV. COMPARISON WITH DATA

Results found for the elastic scattering of 65 MeV protons from ^{118}Sn and of 200 MeV protons from ^{120}Sn have been found from optical potentials formed by folding the effective interactions for those energies that were used previously with much success for data analysis of many nuclei [16], with the densities for the Sn isotopes discussed above and also with the densities of those nuclei specified by a simple $0\hbar\omega$ oscillator model. The oscillator length was taken as $A^{1/6}$; i.e. 2.215 and 2.221 fm, respectively, for the two isotopes. Those results found using the SLy4 and SkP model densities are shown in the following figures by the solid and dashed curves respectively. Those obtained using the HO model densities are portrayed by the dot-dashed curves.

The differential cross sections and analyzing powers for the elastic scattering of 65 MeV protons from ^{118}Sn, measured at the RCNP, Japan [26], are compared with our predictions in Fig. 13. In the case of the differential cross section, there is little difference ($\sim 1\%$) between the SLy4 (solid) and SkP (dashed) results. The calculated results are in good agreement with the structure and magnitude of the data; the SLy4 and SkP model results particularly so. The preference for the SLy4 (SkP) model also is evident with the total reaction cross section. They predict 1.48 b while the HO calculation yields 1.41 b. The measured value [27] is 1.535 ± 0.047 b. But it is with the analyzing power at 65 MeV that the SLy4 (SkP) densities give a significantly better result in comparison to the HO model one. While the HO result is a fair reproduction of the data structure, the SLy4 (SkP) model result gives not only the correct location of the maxima and minima but also shows the overall trend seen in the data of increasing positive in magnitude with increasing angle. They also depict best the marked asymmetry of each peak structure of the data.

The 200 MeV scattering results from ^{120}Sn are also quite good, although with the exception of the differential cross section produced using the HO model the reproductions of data obtained with the mean-field model densities are not as good as found at 65 MeV for ^{118}Sn. The differential cross sections and analyzing powers are shown in Fig. 14 from which it is clearly evident that the HO model tracks the measured data [28] well for all angles shown. The SLy4 model result is not as good, though it agrees with the forward angle ($< 30°$) scattering data well enough. The SkP model result is indistinguishable from the SLy4 one on this scale. The actual differences in cross section are less than a percent at most scattering angles. Both the SLy4 and SkP model calculations thus overestimate the cross section and predict sharper structure than seen in the data for larger scattering angles. Such discrepancies have been noted in other circumstances, notably in a comparative study [15] of model structures for ^{208}Pb and in identifying ^{6}He and ^{11}Li as nuclei with extended neutron distributions (neutron halos) [29, 30]. For this energy the SLy4, SkP and HO calculations gave total reaction cross sections of 1.18, 1.17 and 1.14 b respectively. To compare there is a value measured at 221 MeV [31] (from ^{118}Sn however) of 1.18 ± 0.03 b. As with the differential cross section results, our predictions for the analyzing powers (shown

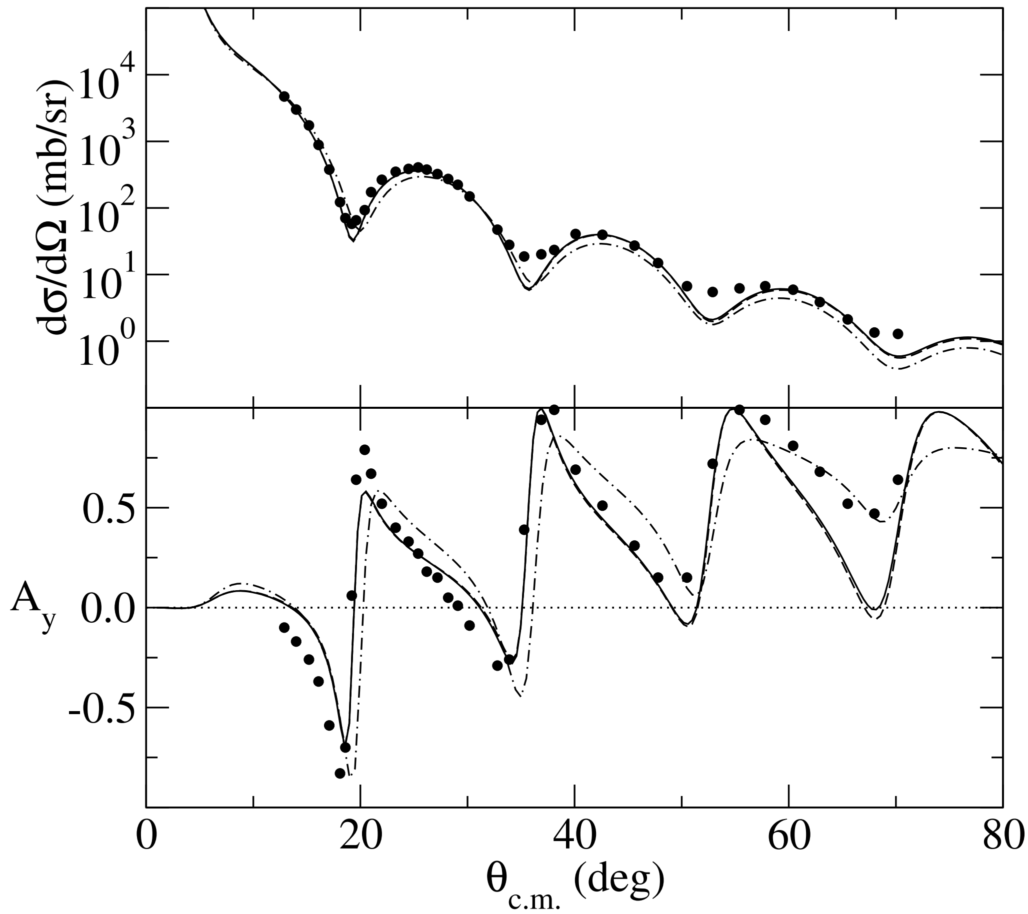

FIG. 13: The differential cross sections (top) and analyzing powers (bottom) for the elastic scattering of 65 MeV protons from ^{118}Sn. The data [26] are compared to the results of the calculations made using the SLy4 (solid line), SkP (dashed line) and HO (dot-dashed line) models.

in the bottom half of Fig. 14) are good but there is room for improvement. The asymmetry seen with the 65 MeV data is less severe at this higher energy but, of course, there are more peaks within the scattering angle range shown. Both features are evident in the HO and SLy4 calculations without the exact angular structures in the data being reproduced. It is notable that the SLy4 and SkP results do match the observed peak magnitudes and valley depths very well and the two densities yield slight but noticeable differences in the spin measurable.

V. CONCLUSIONS

We have made predictions of the observables of the elastic scattering of 200 MeV protons from the even-even isotopes of Sn from ^{100}Sn to ^{176}Sn. The model we have used for the structure of the isotopes is a Hartree-Fock-Bogoliubov model using the Skyrme interaction for which two parameterizations have been used. The matter densities obtained from those models show consistent trends: as mass increases from $A = 100$ to 176 the neutron central density increases and a neutron skin emerges. Also, as proton number is fixed, the addition of neutrons not only increases the volume but also engenders a dilution of the proton

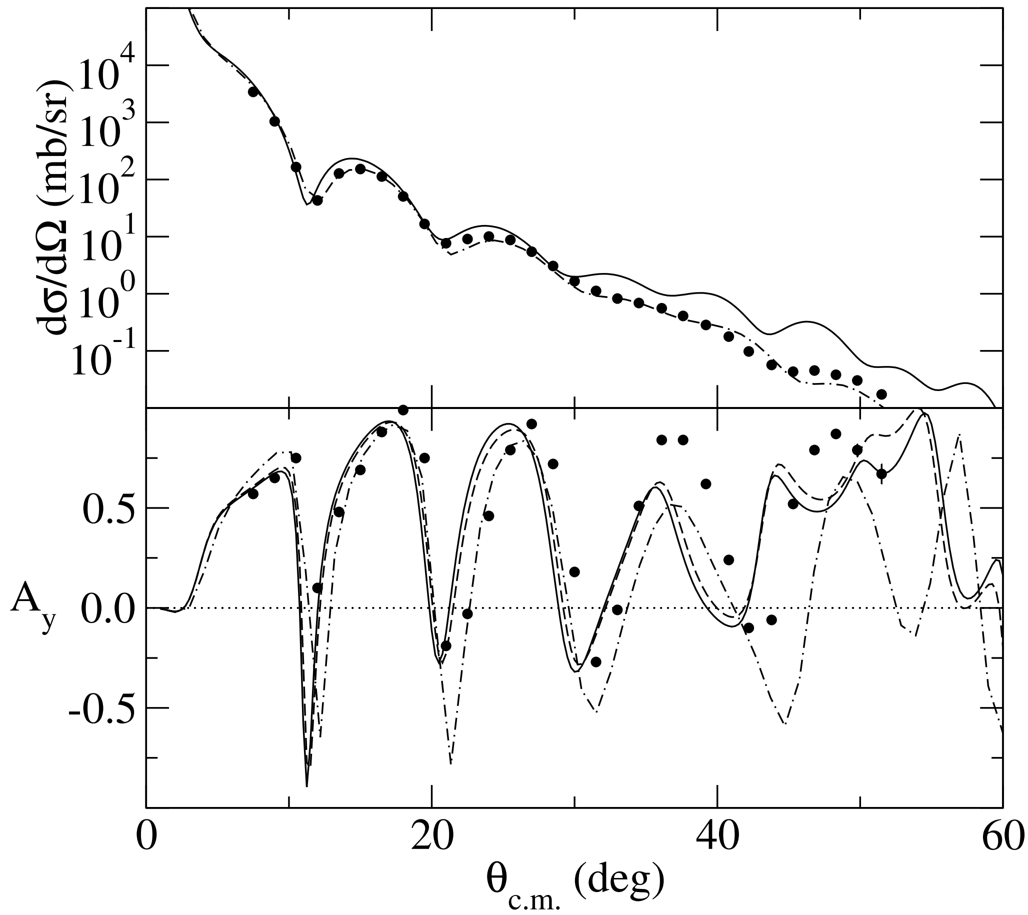

FIG. 14: The differential cross sections (top) and analyzing powers (bottom) for the elastic scattering of 200 MeV protons from ^{120}Sn. The data [28] are compared to the results of the calculations made as given in the text. The curves are as for Fig. 13. The SkP result is not given for the cross section as it is indistinguishable from the SLy4 result.

distribution.

The changes in the neutron density are reflected in the predictions made for the differential cross sections of 200 MeV proton elastic scattering. As neutron number increases, the first three minima tend to lower momentum transfers and the intervening first maximum becomes more pronounced. Such is the effect of the neutron skin as it becomes manifest. There is also some variation in the spin rotation, Q, as mass increases, although those variations are less striking. In the case of ^{118}Sn and ^{120}Sn, comparison with available proton elastic scattering data shows some distinct features: there is very little difference between the densities obtained from the two HFB models considered. While those models do better in the specification of the density of ^{118}Sn in comparison to a naive oscillator model, the predictions for the scattering from ^{120}Sn do not fare as well. This demonstrates the value of comparison to proton elastic scattering data in testing model specifications of the ground states of nuclei.

It is hoped that with the proposed new generation of radioactive beam facilities that data for the elastic scattering of heavy neutron-rich nuclei from hydrogen are obtained. The model we have used in obtaining our predictions is sensitive to the details in the neutron density and serves as an important testing ground for the models being developed to describe such nuclei.

Acknowledgments

This work was supported by a grant from the Australian Research Council, by DOE Contract no. W-7405-ENG-36, and by the Polish Committee for Scientific Research (KBN) under Contract No. 5 P03B 014 21. We also gratefully acknowledge the assistance of Mr. Dirk van der Knijff of the Advanced Research Computing group, Information Division, University of Melbourne not only for use of the high performance computers of that group to find all of the results displayed but also for the technological help to process that data to form the graphs themselves.

[1] P. Hansen, A. Jensen, and B. Jonson, Ann. Rev. Nucl. Part. Sci. **45**, 591 (1995).
[2] E. Roeckl, Rep. Prog. Phys. **55**, 1661 (1992).
[3] A. Mueller and B. Sherrill, Ann. Rev. Nucl. Part. Sci. **43**, 529 (1993).
[4] K. Riisager, Rev. Mod. Phys. **66**, 1105 (1994).
[5] J. Dobaczewski and W. Nazarewicz, Phil. Trans. Roy. Soc. (London) A **356**, 2007 (1998).
[6] S. Mizutori, J. Dobaczewski, G. Lalazissis, W. Nazarewicz, and P.-G. Reinhard, Phys. Rev. C **61**, 044326 (2000).
[7] J. Dobaczewski, I. Hamamoto, W. Nazarewicz, and J. Sheikh, Phys. Rev. Lett. **72**, 981 (1994).
[8] B. D. Serot and J. D. Walecka, Adv. in Nucl. Phys. **16**, 1 (1986).
[9] L. S. Celenza and C. M. Shakin, *Relativistic Nuclear Problem* (World Scientific, Singapore, 1986).
[10] B. A. Nikolaus, T. Hoch, and D. G. Madland, Phys. Rev. C **46**, 1757 (1992).
[11] T. Bürvenich, D. G. Madland, J. A. Maruhn, and P.-G. Reinhard, Phys. Rev. C **65**, 044308 (2002).
[12] P. Ring and P. Schuck, *The Nuclear Many-Body Problem* (Springer-Verlag, Berlin, 1980).
[13] B. A. Brown, Phys. Rev. Lett. **85**, 5296 (2000).
[14] J. Dobaczewski, W. Nazarewicz, and P.-G. Reinhard, Nucl. Phys. **A693**, 361 (2001).
[15] S. Karataglidis, K. Amos, B. A. Brown, and P. K. Deb, Phys. Rev. C **65**, 12345 (2002).
[16] K. Amos, P. J. Dortmans, H. V. von Geramb, S. Karataglidis, and J. Raynal, Adv. in Nucl. Phys. **25**, 275 (2000).
[17] P. K. Deb, K. Amos, S. Karataglidis, M. B. Chadwick, and D. G. Madland, Phys. Rev. Lett. **86**, 3248 (2001).
[18] J. Raynal (1998), computer program DWBA98, NEA 1209/05.
[19] J. Dobaczewski, H. Flocard, and J. Treiner, Nucl. Phys. **A422**, 103 (1984).
[20] J. Dobaczewski, W. Nazarewicz, T. Werner, J.-F. Berger, C. Chinn, and J. Dechargé, Phys. Rev. C **53**, 2809 (1996).
[21] E. Chabanat, P. Bonche, P. Haensel, J. Meyer, and F. Schaeffer, Nucl. Phys. **A627**, 710 (1997).
[22] J. Dobaczewski, W. Nazarewicz, and T. Werner, Physica Scripta **T56**, 15 (1995).
[23] A. H. Wapstra and G. Audi (2001), private communication.

[24] W. Satuła, J. Dobaczewski, and W. Nazarewicz, Phys. Rev. Lett. **81**, 3599 (1998).
[25] R. Machleidt, K. Holinde, and C. Elster, Phys. Rep. **149**, 1 (1987).
[26] M. Yosoi et al. (1985), in RCNP Annual Report, p. 4.
[27] A. Ingemarsson et al., Nucl. Phys. **A653**, 341 (1999).
[28] H. Sakaguchi et al. (1993), in RCNP Annual Report, p. 4.
[29] A. Lagoyannis et al., Phys. Lett. **B518**, 27 (2001).
[30] S. Stepantsov et al., Phys. Lett. (2002).
[31] P. U. Renberg, D. F. Measday, M. Pepin, P. Schwaller, B. Favier, and C. Richard-Serre, Nucl. Phys. **A183**, 81 (1972).